Int. J. Electrochem. Sci., 12 **(2017)** 5772 – 5791, doi: 10.20964/2017.06.80

International Journal of
ELECTROCHEMICAL
SCIENCE
www.electrochemsci.org

Electrocatalytic Behavior of Pt/WO_3 Composite Layers Formed Potentiodynamically on Tungsten Surfaces

Igor A. Pašti[1], *Nemanja M. Gavrilov*[1], *Slavko V. Mentus*[1,2,*]

[1] University of Belgrade, Faculty of Physical Chemistry, Studentski trg 12, 11158 Belgrade, 118, Serbia
[2] Serbian Academy of Sciences and Arts, Knez Mihajlova 35, 11000 Belgrade, Serbia
[*]E-mail: slavko@ffh.bg.ac.rs

Received: 30 January 2017 / *Accepted:* 15 April 2017 / *Published:* 12 May 2017

The Pt/WO_3 composites, in a form of thin layer on W support, were prepared by potentiodynamic polarization of either bare or oxide covered tungsten disc in hexachloroplatinic acid solutions. Both the Pt loading and the thickness of WO_3 interlayer between Pt nanoparticles and W metal surface were varied. The chemical and electrochemical stability tests in 0.1 mol dm^{-3} $HClO_4$ solution were performed by cyclic voltammetry. These test revealed that the shape of cyclovoltammetric curves displayed relatively slight dependence on the number of cycles. The shape changes were attributed to a slight redistribution of WO_3 over the composite surface. Tracking for the synergistic effects in the Pt/WO_3 system, the influence of both WO_3 thickness and Pt loading on the kinetics of both hydrogen evolution/oxidation (HER/HOR) and oxygen reduction reactions (ORR) in acidic solution were investigated. The kinetics of HER was found to be a) independent on the WO_3 thickness, and b) inversely proportional to the Pt loading. For ORR we found that the onset potential, approaching thermodynamic limit of 1.23 V *vs.* RHE, was almost independent on oxide thickness, while the reaction kinetics was commensurable to the Pt loading.

Keywords: platinum, tungsten-oxide, hydrogen oxidation, hydrogen evolution, oxygen reduction

1. INTRODUCTION

Electrocatalysis plays a prominent role in many technological and energy conversion processes, and platinum is one of the bests and most widely used electrocatalysts. For instance it is widely used to catalyse both ORR and hydrogen oxidation reaction (HOR) in low temperature fuel cells. To save platinum, many attempts including formation of either nanodispersed alloys or nanodispersed composites with oxides of transition metals were published [1-4]. In some cases, such as platinum

supported by hypo-d-electronic transition metal oxides is, synergistic effect enhancing catalytic effectiveness was observed [4]. The synergy manifested itself through a specific phenomenon called spill-over, consisting in surface diffusion of adsorbed reactant atoms between platinum and supporting solid phase. This effect was observed particularly for hydrogen evolution reaction (HER), HOR and ORR [5-11]. A known disadvantage of platinum catalyst in fuel cells is its sensitivity to poisoning by CO. The interest for Pt/WO_3 composite arose after discovery that it is more tolerant to the presence of CO in cathode gas than pure platinum [10-13]. Tungsten shows multivalent states which is the necessary prerequisite for spill-over phenomenon. However, the electronic conductivity of tungsten-oxides depends on the oxidation state, the highest one, WO_3, being non-conductive [4]. Moreover, tungsten oxides are soluble in acids and alkalis which can lead to a loss of the active mass [14,15]. Fundamental interactions in Pt/WO_x systems can be linked to Pt /WC catalyst systems, which are important from both experimental [16-19] and theoretical aspects [20-22]. The propensity of WC toward oxidation leads to the formation of WO_3 on WC catalyst surface [23,24]. There is an opinion that a pronounced HER/HOR activity of WC-supported Pt catalyst is just due to the hydrogen spill-over on partially oxidized WC [21].

Since a practical application of oxide-supported metal catalysts demands nanoscopic dispersion of catalytically active component over highly dispersed support, the problems in the interpretation of the results might arise due to the difficulties in the control of catalyst nanoparticles size and their distribution over the support. On the other hand, electrochemical deposition of catalytically active metals over oxidized massive metallic surfaces enables, possibly, the most straightforward way to investigate metal/metal-oxide interactions on a fundamental level, and such kind of composite electrode surface can be considered, in a certain sense, as a model ones. This approach has been previously demonstrated for Pt [25], Ag [26], Au [27] and Pd [28] interaction with TiO_2.

The theoretical and practical importance of Pt/WO_3 composite in electrocatalysis, enlighted in this short literature survey, incited us to investigate the electrocatalytic behavior of this composite in more detail, under improved control of its morphology. In previous studies, usually, Pt/WO_3 composite catalyst was synthesized by either pulse-polarization or temperature induced coprecipitation, from the solutions containing Pt salt and colloidal tungstic acid [10-13], disabling precise control of morphology of the Pt/WO_3 boundary. In this work, Pt/WO_3 composite was formed by a particular procedure, namely, by potentiodynamic polarization of metallic tungsten surface in the solution of hexachloroplatinic acid. This method, already applied by us in other systems [25-28], enables fair control of both morphology and composition of catalyst layer. Namely, nearly spherical Pt particles were obtained, embedded in, or attached on WO_3 oxide layer. The Pt loading and the thickness of the oxide layer were varied. The stability of the electrochemical performance of the composite layer was evidenced by prolonged potentiodynamic cycling. Then, the role of both Pt loading and oxide layer thickness in catalytic activity towards HER/HOR and ORR were investigated. The results revealed the actual level of synergy in the Pt/WO_3 composite in both HER/HOR and ORR electrocatalysis in acidic media.

2. EXPERIMENTAL

2.1. Electrochemical instrumentation

Standard glass three-electrode electrochemical cell equipped with Pine rotator was used. As a counter and a reference electrode, Pt foil and Saturated Calomel Electrode (SCE) were used, respectively. Working electrodes were thin layer composite Pt/WO_3 disk electrodes. For electrochemical formation of composite electrodes on polished polycrystalline tungsten (Alfa Aesar, 99.95%) surfaces, as well as for their electrochemical characterization, Gamry PCI4/750 galvanostat/potentiostat was used. Atmosphere was controlled by blowing high purity gasses (N_2, H_2 or O_2, Messer, 99.9995 vol.%) through the electrolytic solution.

2.2. Electrode preparation and characterization

The morphological and compositional varieties of the Pt/WO_3 working electrodes were prepared on polycrystalline W disk electrode (surface area 0.079 cm^2) mounted in a Teflon holder. The W disk was mechanically polished using grinding paper, washed with ethanol, dried and subjected to electrochemical formation of Pt/WO_3 composite. Five thin layer composite electrodes were prepared, differing in the Pt loading and in the thickness of WO_3 interlayer separating Pt particles from W surface.

A series of composite surfaces with different Pt loading was obtained by potentiodynamic polarization of clean polished W surface in Pt plating solution 0.1 mol dm^{-3} $HClO_4$ + X mol dm^{-3} H_2PtCl_6, performing 25 polarisation cycles between -0.27 V and +1.00 V vs SCE, at 50 mV s^{-1} scan rate. Starting first cycle at -0.27 V (where oxide formation was inhibited) immediately upon W immersion, the initial nuclei of Pt were formed on initially naked W surface, resulting in zero distance between Pt particles and W metal surface. Using three descending concentration of plating solution (X $=1.8\times10^{-3}$, 0.9×10^{-3} and 0.045×10^{-3} mol dm^{-3} H_2PtCl_6), three composite Pt/WO_3 electrodes with descending Pt-loadings (450, 205 and 117 μg cm^{-2}) were obtained with Pt spheres embedded into WO_3 layer, labeled as Pt/WO_3(0)-450, Pt/WO_3(0)-205 and Pt/WO_3(0)-117.

A couple of composite electrodes differing in thickness of WO_3 layer between Pt particles and W surface, was synthesized starting with the oxidized W surface. Namely, by ten potentiodynamic polarization cycles of polished W surface in pure supporting 0.1 mol dm^{-3} $HClO_4$ solution, at a scan rate 50 mV s^{-1}, between - 0.27 and +1.00 V, and between -0.27 and +2.00 V vs SCE, thinner and thicker WO_3 layer, labeled by 1 and 2, respectively, were formed over W surface. Then, by 25 potentiodynamic cycles in 0.1 mol dm^{-3} $HClO_4$ + 1.8×10^{-3} mol dm^{-3} H_2PtCl_6 solution, between -0.27 V and +1.00 V vs SCE at a scan rate 50 mV s^{-1}, Pt-microbeads were grown over the oxide layers. The Pt/WO_3 composite layers labeled as Pt/WO_3(1)-480 and Pt/WO_3(2)-625 were obtained, where the figures within the parentheses symbolize WO_3 layer thickness, and the accompanied three-figure numbers denote the Pt loadings in units g cm^{-2}.

The way of determination of oxide thickness and Pt loadings is discussed later in the Results and Discussion section.

After platinization, the electrodes were washed in deionized water and transferred into the cell filled by the de-aerated electrolyte (0.1 mol dm^{-3} $HClO_4$), in order to perform cyclovoltammetric and RDE measurements.

Scanning electron microscope (SEM) JEOL JSM 6460 LV was used to characterize the morphology of the obtained Pt/W-WO_x composite surfaces.

2.3. Electrochemical measurements

Electrochemistry of tungsten and blank cyclic voltammograms of composite electrodes in acidic solution were investigated using cyclic voltammetry in quiescent N_2-purged 0.1 mol dm^{-3} $HClO_4$. Measurements were done at a common potential sweep rate of 50 mV s^{-1}. HER was investigated using linear sweep voltammetry in the same solution at a potential sweep rate of 10 mV s^{-1}. HOR and ORR were investigated using voltammetry on rotating disk electrode (RDE) in H_2 and O_2-saturated supporting electrolyte, respectively. HOR polarization curves were recorded at scan rate of 10 mV s^{-1} while ORR polarization curves were collected at 20 mV s^{-1}. *I-E* curves related HER, HOR and ORR catalysis on composite electrodes were recalculated with respect to Reversible Hydrogen Electrode scale (RHE), in order to enable easier comparison with the literature data. For this purpose potential difference (determined as open circuit potential) between the SCE reference electrode and the RHE electrode formed in the used $HClO_4$ electrolytic solution (achieved by purging H_2 over platinized Pt mash electrode) was used. Measured currents were corrected for Ohmic drop (iR drop) using uncompensated solution resistance determined by AC impedance.

3. RESULTS AND DISCUSSION

3.1 Potentiodynamic formation of Pt/WO_3 composite layer on W surface

3.1.1 Potentiodynamic oxidation of tungsten surface in pure supporting electrolyte

Tungsten displays very rich pH-dependent electrochemistry, characteristic of different oxidation and dissolution kinetics in highly acidic and highly alkaline solutions. Upon anodic polarization of tungsten in alkaline solution, a series of non-stoichiometric tungsten oxides, namely $WO_{2.72}$, $WO_{2.90}$ and $WO_{2.96}$ appear, preceeding the formation of WO_3 [29]. At very deep anodic potentials, anodic dissolution takes place, described by Kelsey [30] by the reaction

$$W + 8OH^- \rightarrow WO_4^{2-} + 4H_2O + 6e^- \quad (1)$$

In acidic solution, anodic oxidation of tungsten leads directly to the formation of WO_3 layer. In concentrated acids, WO_3 may be dissolved chemically with the participation of protons as reactants [14, 31]:

$$WO_3 + H^+ \rightarrow WO_2OH^+ \quad (2)$$

The reaction (1) is much faster than the reaction (2) [14, 31].

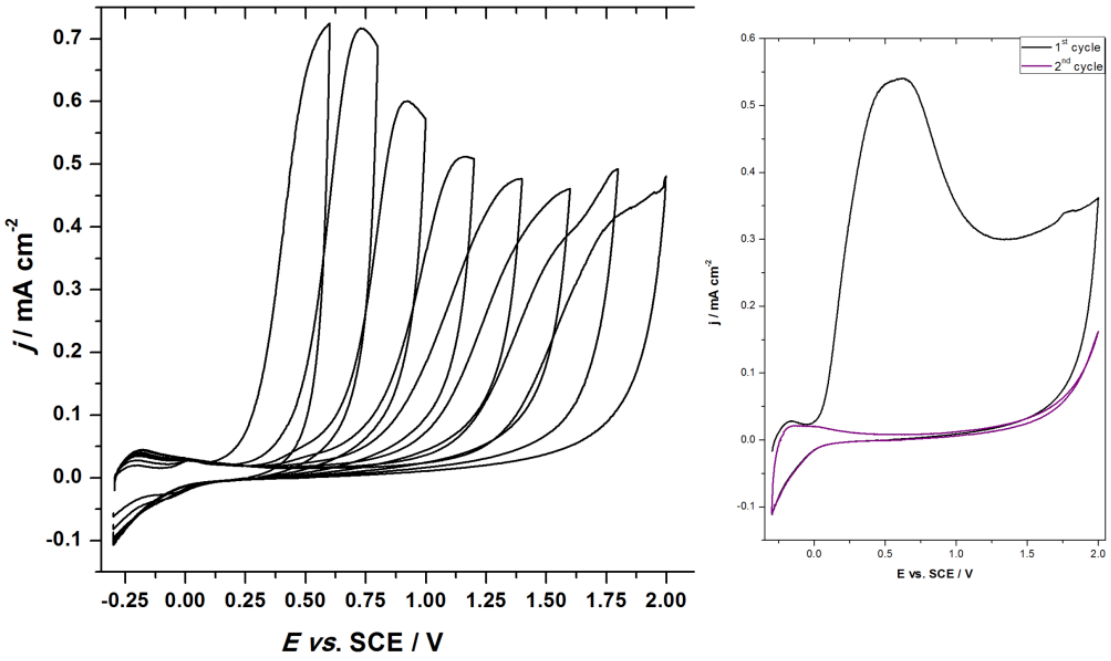

Figure 1. Series of cyclic voltammogram of polished W disc in 0.1 mol dm^{-3} $HClO_4$ solution obtained upon progressive extension of vertex anodic potential (left). Right: first (black line) and second (pink line) potentiodynamic cycle of W disc obtained with a common vertex anodic potential of 2 V *vs.* SCE in the same solution. Potential scan rate was 50 mV s^{-1}.

In the cyclic voltammetry experiments in 0.1 mol dm^{-3} $HClO_4$ solution, performed in this study, upon reversal of polarization direction from anodic to cathodic one, the current suddenly droped to nearly zero (Fig. 1), indicating passivation of the surface [14]. Regardless of the number of polarization increments, the oxide thickness is function of the vertex anodic potential, and, as shown in Fig 1, right, the oxide layer achieves its maximum thickness (dependent on final anodic potential) already during the first polarization cycle. Passive oxide layer formed in the first cycle prevents the oxide thickening in the following cycles, if previously achieved vertex anodic potential is not exceeded. This behavior is characteristic of a group of so called "valve" metals [25], to which tungsten also belongs. For a known molar mass M, valence z, oxide density δ_{ox}, the oxide layer thickness, d, is defined by the number of coulombs Q_{ox}, consumed for oxide formation, which may be determined by integrating the anodic part of the cyclovoltammogram [25] :

$$d = \frac{MQ_{ox}}{zF\delta_{ox}} \quad (3)$$

For valve metals, the number of coulombs consumed for oxide formation is dependent exclusively on the vertex anodic potential.

Relatively small cathodic current observed in the region of vertex cathodic potential stems from the formation of hydrogen-tungsten bronze [12, 33] according to the equation:

$$WO_3 + xH^+ + xe^- \rightarrow H_xWO_3 \qquad (0 < x < 1). \qquad (4)$$

The two stable forms of hydrogen tungsten bronzes, namely $H_{0.18}WO_3$ and $H_{0.35}WO_3$ and also substoichiometric tungsten oxide:

$$WO_3 + xH^+ + xe^- \rightarrow WO_{3-\frac{x}{2}} + \frac{x}{2}H_2O \qquad (0 < x < 1). \qquad (5)$$

were reported [33].

The oxide mass loss, being very small, may not be detected by cyclic voltammetry, however, it was detected by electrochemical quartz microbalance in both anodic and cathodic scan in 0.1 mol dm^{-3} H_2SO_4 supported by 0.4 mol dm^{-3} Na_2SO_4 [32]. Obtained results indicate that it is relatively easy to control the oxide thickness formed on the W surface under potentiodynamic polarization in acidic solution, since it depends exclusively on the vertex anodic potential. This may serve to explain what happened when polished W surface was polarized potentiodynamically in 0.1 mol dm^{-3} $HClO_4$ $+1.8\times10^{-3}$ mol dm^{-3} H_2PtCl_4 solution, as discussed in the next section.

3.1.2. Potentiodynamic polarization of bare and preoxidized W surface in Pt plating solution to synthesize Pt/WO_3 composite

Fig 2. shows the first and the tenth cyclic voltammograms obtained in 0.1 mol dm^{-3} $HClO_4$ $+1.8\times10^{-3}$ mol dm^{-3} H_2PtCl_4 solution used as a Pt plating one, for the following three cases: 1. bare W surface, 2. potentiodynamically preoxidized W surface in 0.1 mol dm^{-3} $HClO_4$ up to the vertex anodic potential 1 V vs SCE, and 3. potentiodynamically preoxidized W surface in 0.1 mol dm^{-3} $HClO_4$ up to the vertex anodic potential 2 V vs SCE, starting always at -0.27 V vs SCE. As obvious, in plating solution, the current is cathodic one in almost complete potential region, and leads to a progressive growth of platinum beads, the nuclei of which were formed at very start of the potential cycling.

In the case #1, oxide layer grew simultaneously with the formation and growth of Pt nuclei, and was completed already within the first cycle to the thickness corresponding to the vertex anodic potential of 1 V. The polarization cycles were then continued up to 25 ones in total, when exclusively Pt beads grew in positions of initially formed nuclei. The growth of Pt particles may be controlled visually by mediation of the surface of hydrogen adsorption/desorption peaks in the potential region -0.27 to +0.2 V. This way of synthesis yielded the composite in which platinum beads, imbedded into thin WO_3 layer, contacted directly to W metal. This composite is labeled as Pt/WO_3(0)-450 (zero within parentheses denotes zero distance between Pt beads and W surface, 450 being the Pt loading in μg cm^{-2} units).

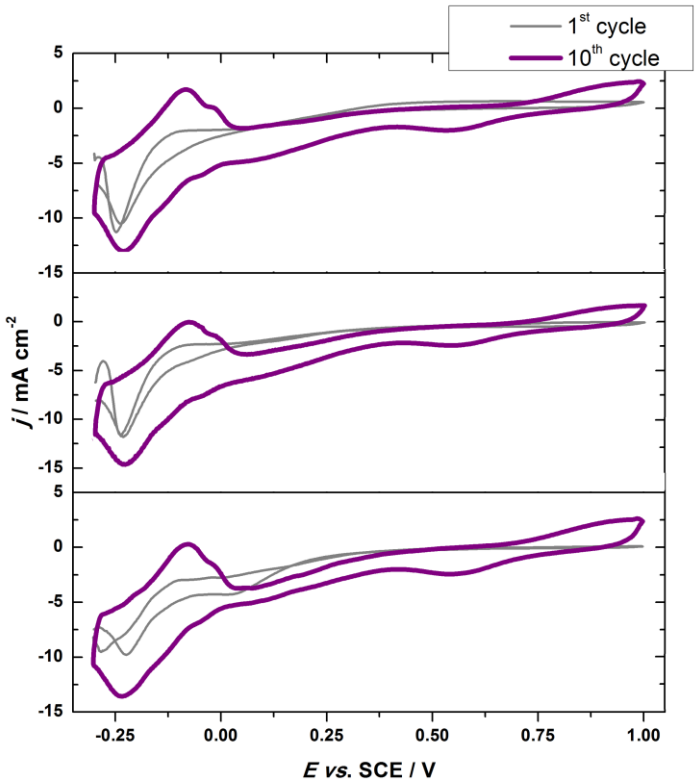

Figure 2. The first (thin line) and the tenth (thick line) cyclic voltammograms of platinization of W (top) or WO_3/W surfaces in 0.1 mol dm^{-3} $HClO_4$ +1.8×10^{-3} mol dm^{-3} H_2PtCl_4 solution at 50 mV s^{-1} (initial surface state: top – naked W , middle – WO_3(2V)/W, bottom – WO_3(1V)/W

Repeating the procedure described as the case #1, in subsequently halved concentration of plating solutions, the composite layers with decreasing Pt loading were obtained, labeled as Pt/WO_3(0)-205 and Pt/WO_3(0)-117.

In the two following cases, the WO_3 layers, the thickness of which corresponded to the vertex anodic potential of 1V and 2 V, respectively, were used as the supports on which Pt nuclei were grown during 25 potentiodynamic cycles in plating solution 0.1 mol dm^{-3} $HClO_4$ +1.8×10^{-3} mol dm^{-3} H_2PtCl_4. These Pt/WO_3 composites are labeled as Pt/WO_3(1)-480 and Pt/WO_3(2)-625 (thinner, 1, and thicker, 2, WO_3 layer, distancing Pt beads from W metal surface, and their Pt loadings were 480 and 625 μg cm^{-2}). Although intended to be constant, the Pt loading did not achieve identical values, but scattered somewhat between 450 and 625 μg cm^{-2}.

Pt loadings for all five composite surfaces, reported also in Table I, were evaluated by numerical integration of unfolded potentiodynamic curves of Pt deposition. The contribution of surface processes related to WO_3 formation, according to the ratio of current axis units in Fig's 1 and 2, was relatively small and estimated to be below 2%, causing the error of determination of Pt loading only in the first potentiodynamic cycle.

The inspection of obtained Pt/WO_3 composite electrode surfaces by SEM (Fig. 3) pointed to relatively uniformly sized submicron Pt particles in all three cases. During the growth, certain fraction of Pt particles coalesced and formed larger agglomerates. On the right side a sketch of the Pt bead position relative to the W surface was presented.

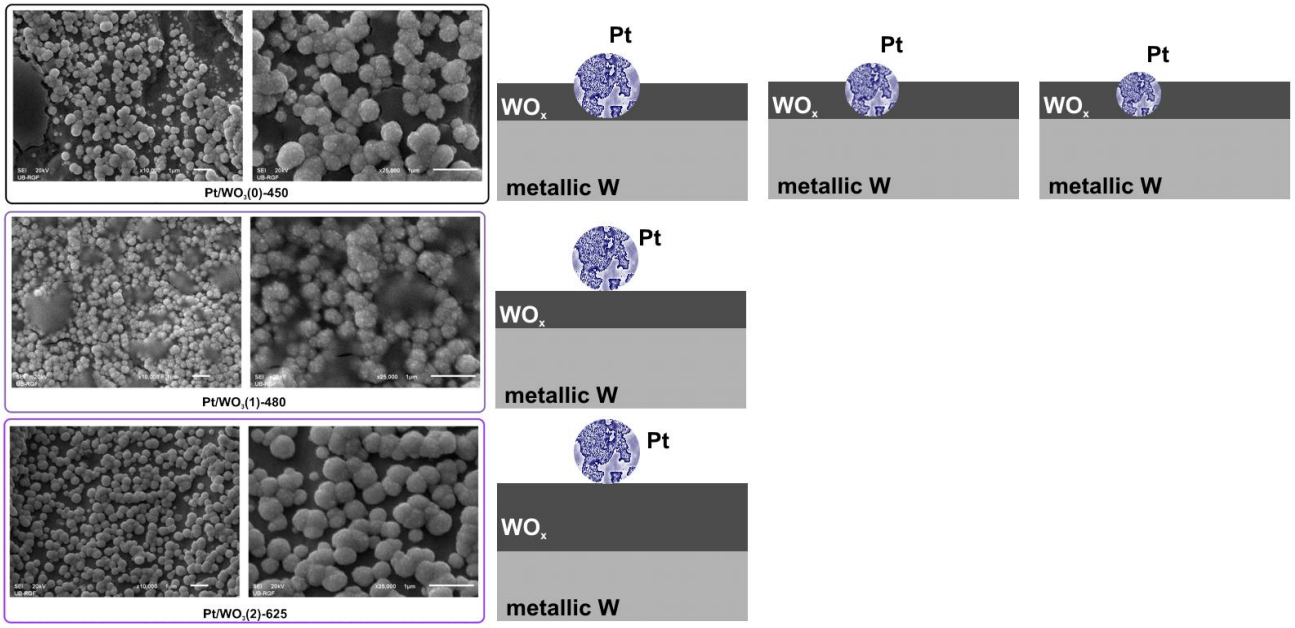

Figure 3. SEM micrographs of Pt-WO_3 composite on tungsten surfaces: top – Pt/WO_3(0)-450; middle – Pt/WO_3(1)-480, bottom – Pt/WO_3(2)-625. On the right hand side, schematic illustration of Pt microbead position with respect to WO_3 support is provided. (In the drawn schemes, the oxide thickness is exaggerated to outline differences between composites)

3.2. Cyclic voltammetry of composite Pt/WO_3 surfaces in 0.1M $HClO_4$ solution in inert atmosphere

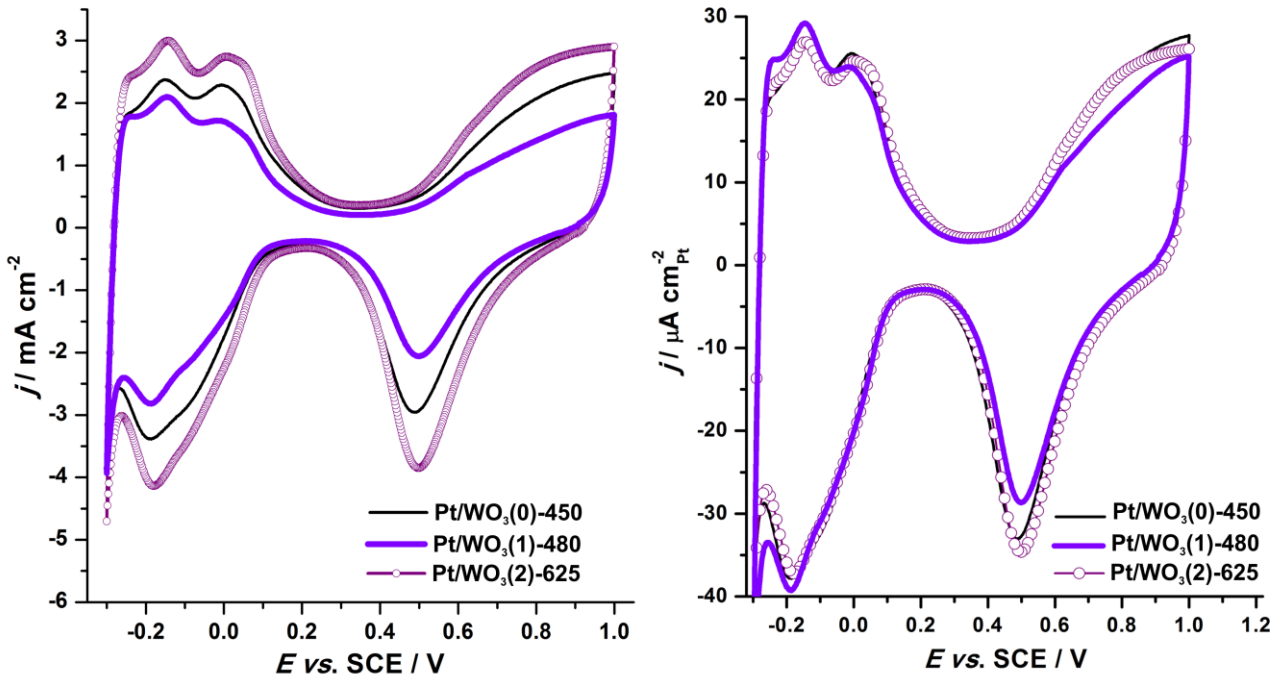

Figure 4. Cyclic voltammograms of Pt/WO_3(0) electrodes: thin line – Pt/WO_3(0)-450; thick line – Pt/WO_3(1)-480, circles – Pt/WO_3(2)-625; normalized per unit of geometrical cross section area (left), and per unit of active Pt surface area (right). Cyclic voltammograms were recorded in N_2-purged 0.1 mol dm^{-3} $HClO_4$ solution at 50 mV s^{-1}.

Blank cyclic voltammetry of prepared Pt/WO_3 composite electrode surfaces, in a series with different Pt-W distances, recorded in N_2-purged 0.1 mol dm^{-3} $HClO_4$ solution, reflected somewhat scatter in the amounts of Pt deposited across, or over, WO_3 layer (Fig. 4, left). In Fig 5 the cyclovoltammograms recorded under the same conditions, for the Pt/WO_3 composite series with various Pt loading: Pt/WO_3(0)-450, Pt/WO_3(0)/205 and Pt/WO_3(0)-117 is presented.

The basic shape of cyclovoltammogram of platinum surface in acidic solution, with clearly distinguishable fine structure in the regions of both hydrogen and oxygen adsorption/desorption, related to the energetic heterogeneity of the surface of polycrystalline Pt, well known from the literature [12,26], is somewhat smoothed in the studied examples. The loss of fine structure causes WO_3, particularly in the region of hydrogen adsorption/desorption, where simultaneously hydrogen bronze H_xWO_3 formation/ disintegration takes place, as clearly demonstrated by Jayaraman et al. [12]. Interestingly, the amount of Pt deposited on WO_3 electrode surface under identical conditions was found to be commensurate to the WO_3 thickness. (Table 1).

By integration the parts of cyclic voltammograms corresponding to the hydrogen underpotential deposition (H_{UPD}), electrochemically active surface area (*ESA*) was evaluated, which enabled further evaluation of Pt specific surface area (S_{Pt}). Obtained data indicate relatively similar S_{Pt} for all three composite electrode surfaces (Table 1). When recorded cyclic voltammograms were evaluated with respect to *ESA* (Fig. 4 right, and Fig. 5, right) it was observed that kinetics of surface process discernible on cyclic voltammograms is not largely affected by the WO_3 thickness and Pt loading, at least inside of their limits studied here. However, it appears that kinetics of Pt oxidation/Pt-oxide reduction on the Pt/WO_3(0)-450 composite layer is somewhat hindered, compared to other two cases.

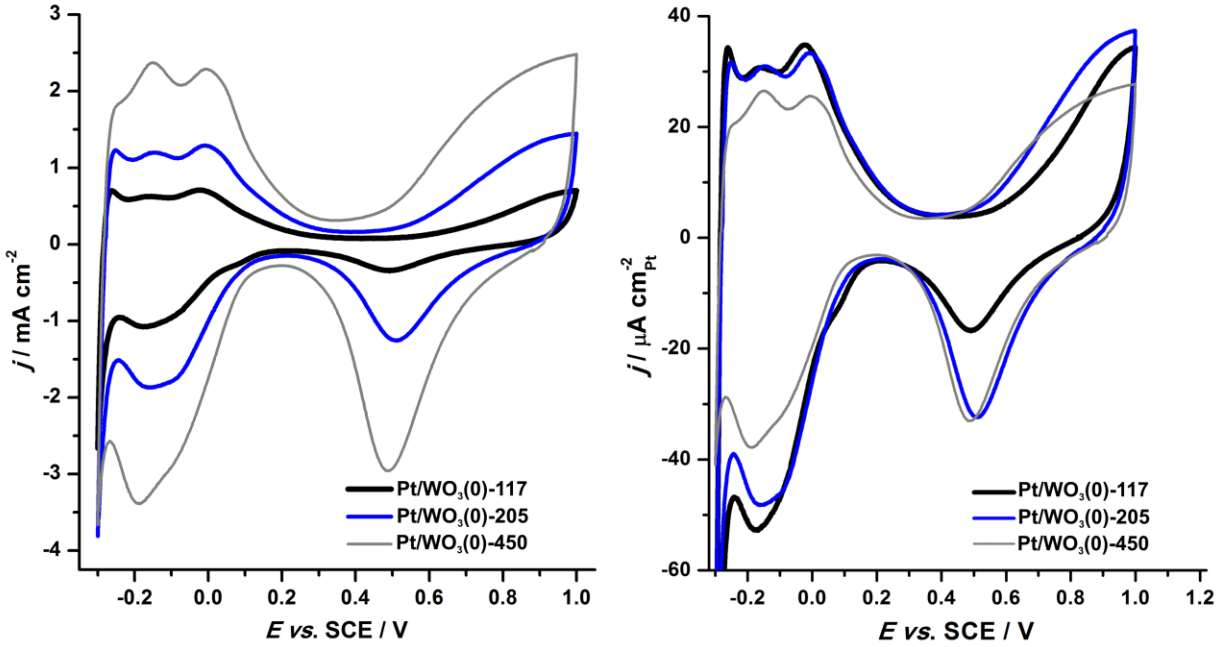

Figure 5. Cyclic voltammograms of composite Pt/WO_3 with variable Pt loading Pt/WO_3(0)-450 (thin line), Pt/WO_3(0)-205 (thick blue line), Pt/WO_3(0)-117 (thick black line), normalized *per* unit of geometrical cross section area (left) and Pt surface area (right). Cyclic voltammograms were recorded in N_2-purged 0.1 mol dm^{-3} $HClO_4$ solution at 50 mV s^{-1}

It is interesting to compare cyclic voltammograms of Pt/WO_3 composite electrode presented here, against those of the potentiodynamically formed Pt/ TiO_2 composite reported previously [25]. In the latter case, the Pt loading was determined to be approximately a half of the ones reported here, while S_{Pt} was basically the same. This indicates that on TiO_2 surface formed over metallic Ti in a manner similar to that used here, Pt is more finely dispersed, which agrees with the morphology of Pt deposit over TiO_2 [25]. Moreover, cyclic voltammograms of Pt/TiO_2 composite electrodes provide much better resolution of surface process occurring on Pt in the investigated potential window, resembling to the cyclic voltammogram of polycrystalline Pt (pc-Pt).

Table 1. Evaluated Pt loading (L(Pt)), hydrogen adsorption/desorption charge ($Q_{H_{UPD}}$), electrochemical surface area (*ESA*) and corresponding Pt specific surface area (S_{Pt}) of differently prepared Pt/WO_3 composite surfaces.

Pt/WO_3	***L*(Pt) / mg cm^{-2}**	**$Q_{H_{UPD}}$ / mC cm^{-2}**	***ESA* / cm^2**	**S_{Pt} / m^2 g^{-1}**
Pt/WO_3(2)-625	0.625	22.9	8.78	17.5
Pt/WO_3(1)-480	0.480	14.8	5.67	14.7
Pt/WO_3(0)-450	0.450	18.5	7.07	19.5
Pt/WO_3(0)-205	0.205	7.98	3.06	18.5
Pt/WO_3(0)-117	0.117	4.21	1.61	17.1

3.3. Stability of Pt/WO_3 composite surfaces underwent to a potentiodynamic cycling

As pointed out in the introduction, stability issue of tungsten-oxide species under electrochemical conditions are linked not only to the operation of oxide-containing catalysts, but also to the performance of WC-supported PEMFC catalysts, which is in the focus of current research [23,24]. On the other hand, the approach demonstrated here to prepare catalytically active Pt/WO_3 surfaces enables relatively easy assessment of the stability of W-oxide containing Pt-based catalysts. For this purpose we applied extended potentiodynamic cycling of Pt/WO_3-450 electrode prepared by platinization of polished W disk. Upon extended cycling (n > 50) cyclic voltammogram starts to evolve and certain peculiarities can be observed (Fig. 6). First noticeable changes are observed in hydrogen adsorption/desorption region. H deposition peak suffers only a small change in intensity starting from 0.05 V *vs*. SCE (around 10 % in total). However, H desorption peaks lose their structure and become distorted towards more positive potential. The most striking change is observed in Pt oxidation region where both anodic and cathodic responses are cut down to a half of that before cycling. Similar cyclic voltammograms can be found in the work presented by Martínez et al. [34] for the case of potentiostatically and potentiodynamically deposited tungsten-oxo species over pc-Pt

surface. The authors concluded that such electrochemical response of W-modified Pt electrode is due to the presence of W(VI)/W(V) surface redox couple and the half-reaction:

$$WO_4^{2-} + e^- \Leftrightarrow WO_4^{3-} \quad (6)$$

In fact, it was proposed that the distorsion of electrochemical response of such electrode in H_{UPD} region is due to the reaction (6), not only due to the H deposition/desorption. However, it is interesting to observe that total charge associated to the voltammetric peaks in the H_{UPD} on clean Pt-poly and W-oxo-modified pc-Pt are quite similar [34]. It was suggested that tungsten-oxo anion blocks water discharge in standard Pt-oxide formation region, what has also the consequence to ORR, see Fig. 10. It should be noted that WO_3 dissolution is one of the main disadvantages of Pt/WO_3 catalysts, as observed some time ago by Tseung et al.[15], and the attempt to prevent the dissolution of the support, proposed by the authors consists in the coating of electrode surface by a thin nafion layer.

By combining obtained results and previous reports it can be concluded that, upon extended cycling, W-oxo species dissolved at deep anodic potentials from WO_3 surface get deposited at Pt particles during cathodic excursions. This is, however, the only effect while the progressive loss of Pt, which would be reflected in large decay of current response in H_{UPD} region, was not observed.

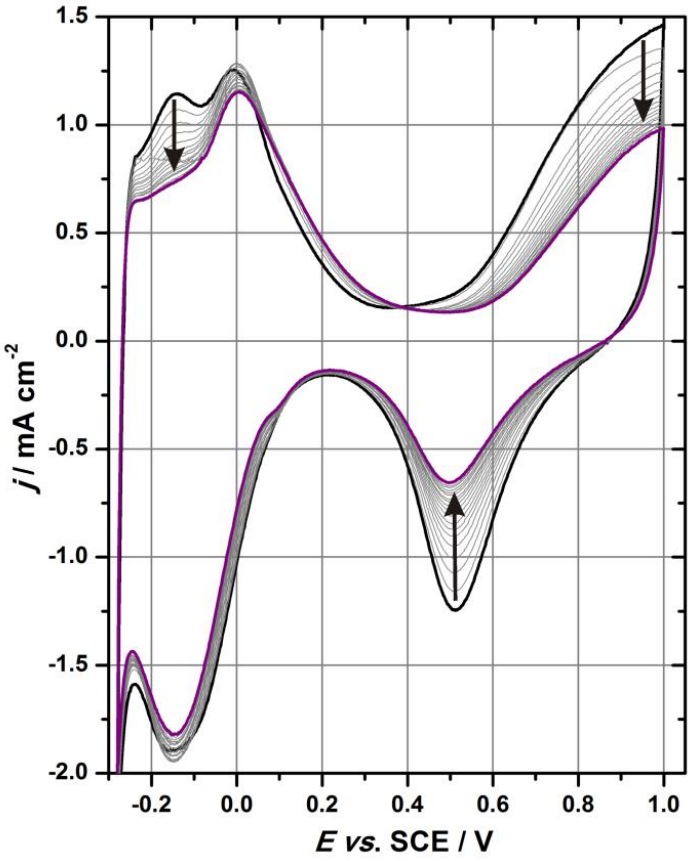

Figure 6. Changes of a blank cyclic voltammogram of Pt/WO_3 electrode upon extended potential cycling in N_2-purged 0.1 mol dm^{-3} $HClO_4$ (potential scan rate was 50 mV s^{-1}, Pt loading was set to 0.2 mg cm^{-2}). The arrows indicate the direction of shape change on cycling.

3.4. Electrocatalysis of HER/HOR on Pt/WO_3 composite electrodes

3.4.1. The influence of WO_3 thickness

HER kinetics, probed in quiescent $HClO_4$ solution, points that prepared Pt/WO_3 composite electrode surfaces are highly active for this electrocatalytic reaction (Fig. 7, left). Normalization of HER polarization curves with respect to ESA indicated that among prepared composite electrode surface the most active one was Pt/WO_3(0)-450.

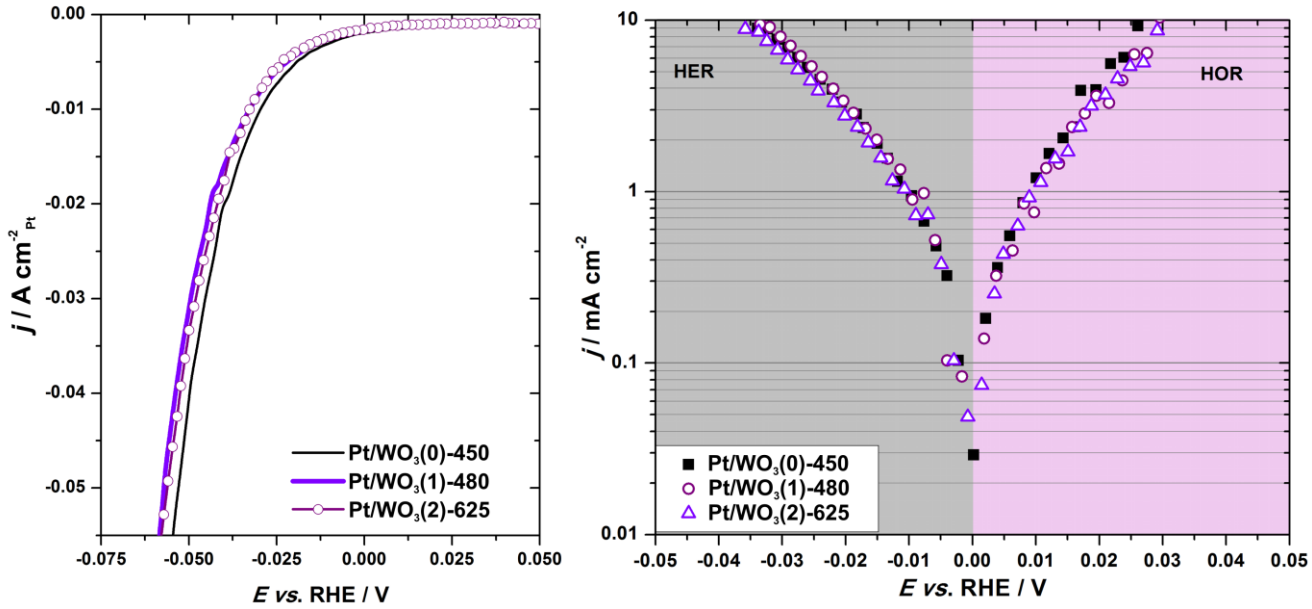

Figure 7. Linear sweep voltammograms of HER on composite surfaces: Pt/WO_3(0)-450, Pt/WO_3(1)-480 and Pt/WO_3(2)-625, normalized *per* Pt surface area (left), and HER/HOR *j-E* curves in log-linear coordinates (normalized *per* geometric surface area) (right). HER curves were recorded in quiescent N_2-purged 0.1 mol dm^{-3} $HClO_4$ solution at 10 mV s^{-1}. HER/HOR curves were recorded in H_2-saturated 0.1 mol dm^{-3} $HClO_4$ solution at 10 mV s^{-1} using RDE technique (ω = 1400 rpm). HOR branch was corrected for mass transfer limitations by means of Kuotecky-Levich equation.

Under experimental conditions, diffusion limitations are difficult to reach in the case of HER, but this is not the case for HOR. Limited H_2 solubility in $HClO_4$ affects the measured current density (j) under RDE conditions by mass transport limitations according to the Koutecky-Levich equation [35]:

$$\frac{1}{j} = \frac{1}{j_k} + \frac{1}{j_d(\omega)} = \frac{1}{j_k} + \frac{1}{B \cdot \omega^{\frac{1}{2}}} \qquad (7)$$

In this equation j_k and $j_d(\omega)$ stand for kinetic current density and limiting diffusion current density, the later one being a function of a electrode rotation rate (ω). The constant B assembles the number of transferred electrons, solubility of H_2, its diffusivity (measured as diffusion coefficient) and

kinematic viscosity of a solution. Hence, j_k (which expresses charge transfer kinetics) can be extracted as:

$$j_k = \frac{j \cdot j_d}{j_d - j} \quad (8)$$

in order to correct for mass transfer limitations. This correction is particularly important for this reaction, since, according to Quaino et al. [36], diffusion limitations manifest themselves even at 0.0 V vs RHE, and at high rotation rates. Upon such correction kinetic current densities for HER and HOR on these three electrodes have been mutually compared (Fig. 7, right), which pointed out to the symmetry of HER and HOR branches around reversible electrode potential. Such observation is a confirmation that HER and HOR on these surfaces proceed *via* the same mechanism and intermediates, as diagnosed previously for carbon-supported nanosized Pt catalysts [37]. Tafel slope is traditionally used to diagnose the mechanism of hydrogen electrode reactions based on linear fit of *E vs.* $\log(j_k)$ curve. Here is useful to discuss actual limitations of RDE technique. It measures not the very charge transfer step of HER/HOR, which is very fast (j_0 ~ 100 mA cm^{-2}) but the kinetics of overall process which includes hydrogen adsorption/desorption step [38]. Nevertheless, overall HER/HOR kinetics is rather fast [j_0 ~ 0.1 – 1 mA cm^{-2}] [37, 38] , resulting in diffusion limitations achieved promptly in HOR branch (for the overpotentials above +50 mV) and intensive H_2 formation at low cathode overvoltages. In both cases it was not possible to reach overvoltages high enough for Tafel analysis as in HER branch H_2 oversaturation and bubble formation can introduce mass transport resistances [37] while in HOR branch Eq. (7) can be applied for $j \leq 0.8\ j_d$ (in order to avoid serious artifacts introduced by numerical manipulations of experimental data). It should be noted that presented experimental approach is the standard one in the measuring HER/HOR kinetics and RDE measurements of Pt-based catalysts usually lead to the values as reported here [37]. As discussed by Sheng et al. [37] other approaches such as the use of Pt microelectrodes, gas-diffusion electrodes and fast transient methods [38] could lead to significantly higher exchange current densities, approaching the ones of very charge transfer step. Apparently, diffusion limitations are difficult to remove within the RDE setups. However, it can be safely concluded that HOR/HER exchange current density is in the range of typically observed ones in RDE measurements on Pt catalysts, being between 0.1 and 1 mA cm_{Pt}^{-2} [37-41]

3.4.2. The influence of Pt loading

In order to investigate the effect of Pt loading on electrocatalytic behavior of Pt/WO_3 composite surfaces, the series of electrodes with decreasing Pt loadings was used. Template action of the surface similar to than observed in potentiodynamically formed Pt/TiO_2 [25], preserved similar particle density of Pt particles, but differing in mean radii.

Hydrogen evolution curves were recorded in quiescent N_2-purged 0.1 mol dm^{-3} $HClO_4$ solution at 10 mV s^{-1}. Hydrogen evolution/oxidation curves were recorded in H_2-saturated 0.1 mol dm^{-3} $HClO_4$

solution at 10 mV s^{-1} using RDE technique (ω = 1400 rpm). HOR branch was corrected for mass transfer limitations by means of Kuotecky-Levich equation. In contrast to electrode series when WO_3 thickness has been varied, HER/HOR proceses have shown dependence on Pt loading. When normalized to the unit of ESA, the reduction of Pt loading by a factor of nearly 4, led to one order of magnitude higher activities. As S_{Pt} does not depend significantly on the loading (Table 1), this conclusion holds also for activities expressed in units of mass activity. It is suggested that these peculiarities are direct consequence of spill-over processes, which result in the change of the state of the composite surface according to the reaction:

$$Pt/H_xWO_3 \Leftrightarrow Pt/W(OH)_6 \quad (9)$$

This picture is in line with the observation that the catalytic activity of nanosized Pt/bronze exponentially increases with decreased Pt size approaching maximum at monoatomic dispersion [4]. Under RDE conditions the electrode with the lowest Pt loading still dominates as the most active one (Fig. 8, right) but the relative differences are somewhat diminished under forced convection conditions.

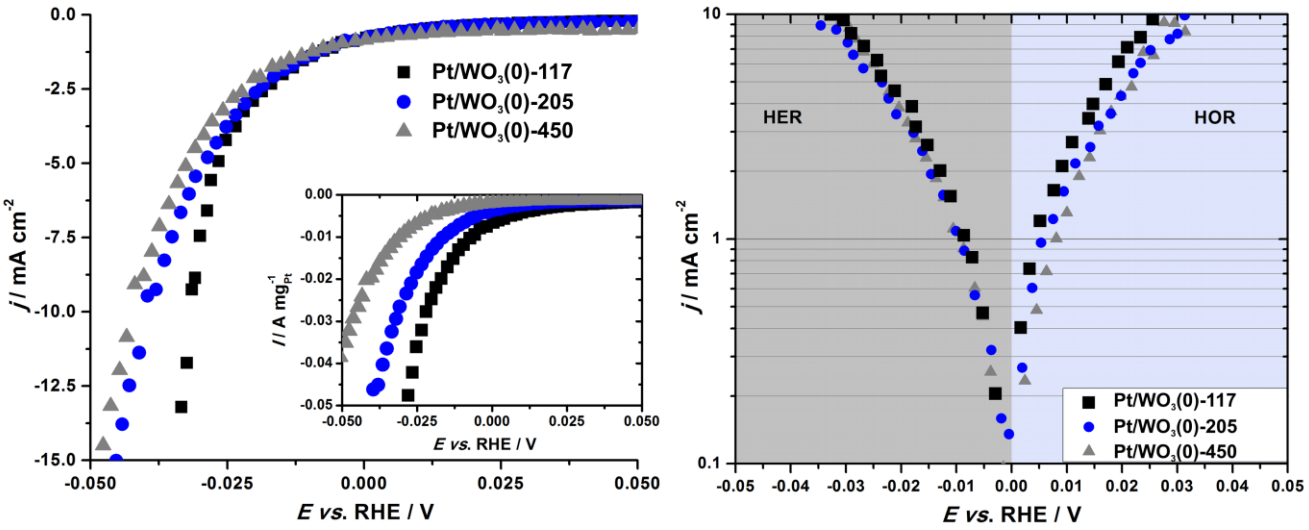

Figure 8. Left: HER linear sweep voltammograms on $Pt/WO_3(0)$-450, $Pt/WO_3(0)$-205 and $Pt/WO_3(0)$-117 composite surfaces, with different Pt loadings, normalized *per* geometrical surface area and Pt loading (inset). On the right HER/HOR *j-E* curves in log-linear coordinates (normalized *per* geometric surface area) are provided. Hydrogen evolution curves were recorded in quiescent N_2-purged 0.1 mol dm^{-3} $HClO_4$ solution at 10 mV s^{-1}. Hydrogen evolution/oxidation curves were recorded in H_2-saturated 0.1 mol dm^{-3} $HClO_4$ solution at 10 mV s^{-1} using RDE technique (ω = 1400 rpm). HOR branch was corrected for mass transfer limitations by means of Kuotecky-Levich equation.

The obtained results can be linked not only to the Pt/WO_3 type of electrocatalysts, but also to the extensively investigated Pt/WC catalysts [16-18]. Namely, it was proposed that improved HER/HOR kinetics, which is often reported for WC-supported nanosized Pt electrocatalysts, compared to Pt/C catalysts, is not due to the electronic effects of the support, but due to the hydrogen spill-over on partially oxidized WC support [21]. In fact, obtained result suggest that the state of the oxidation of

the support and suitable Pt dispersion over the WO_3 support affect HER/HOR kinetics significantly, which can also play role in the performance of Pt/WC electrocatalysts as WC oxidation is rather difficult to avoid [16].

3.5. Electrocatalysis of ORR on Pt/WO_3 composite electrodes

3.5.1 The influence of WO_3 thickness

ORR kinetics is generally much slower than HER/HOR kinetics. The differences in Pt/WO_3 composites produced more pronounced differentiation in ORR than in HER-HOR kinetics (Fig. 9). The most active was Pt/WO_3 (0)-450, then Pt/WO_3 (1)-480 and then Pt/WO_3 (2)-625 composites. It should be noted that measured limiting current densities agree with those for complete $4e^-$ O_2 reduction to H_2O [25]. In comparison to previously reported Pt/TiO_2 composite electrode [25], rather similar ORR activities were observed, altthough direct comparison is somewhat difficult, due to the use of different potential scales and different potentials sweep rates used to obtain Tafel diagrams [31]. The ORR onset potential was observed to be very high, above 1 V *vs.* RHE, which is partially due to high Pt loading, but also points to a high intrinsic ORR activity of Pt/WO_3 composites. For example, the ORR onset potentials observed here are higher compared to the ones obtained under identical conditions on platinized Pt disk [42]. However, upon increasing ORR overpotential, measured current density increases slowly. This resulted in very high values of Tafel slopes (Fig. 9, inset; Table 2).

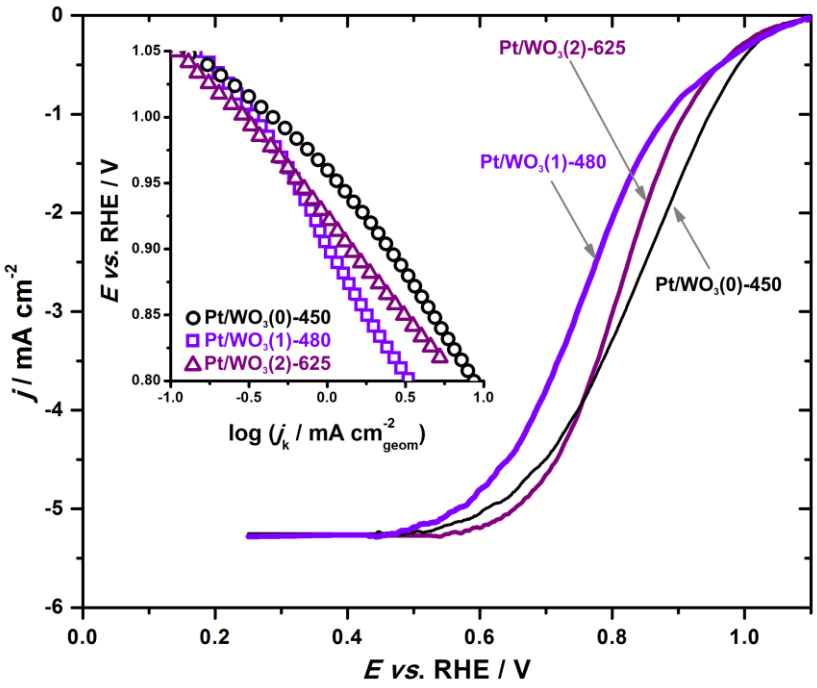

Figure 9. Background-corrected *j-E* curves of oxygen reduction reaction on Pt/WO_3 (0)-450, Pt/WO_3 (1)-480 and Pt/WO_3 (2)-625 composite surfaces recorded in O_2-saturated 0.1 mol dm^{-3} $HClO_4$ solution at 20 mV s^{-1} using RDE technique (ω = 1400 rpm). Inset gives corresponding Tafel plots; currents were corrected for mass transfer limitations.

These values are significantly higher compared to ORR Tafel slopes found on platinum, which are within -60 (low overvoltage region) and -120 (high overvoltage region) mV *per* decade (see ref. [42] for more in-depth discussion). Using the Eq (8) to extract kinetic current density at a specified electrode potential, specific activity (j_{spec}) can be evaluated:

$$j_{spec} = \frac{j_k \times A}{ESA} \tag{10}$$

where *A* stands for the disk geometrical cross section area. Due to high ESA of Pt/WO_3 composite electrodes and high values of Tafel slopes, estimated j_{spec} were found to be approximately one order of magnitude lower compared the state-of-the-area Pt-based ORR catalysts [2] (Table 2).

Table 2. Evaluated ORR Tafel slopes in low and high ORR overpotential regions, followed by ORR specific activities (j_{spec}) evaluated at 0.9 V *vs*. RHE. In the last row the data for high surface area pc-Pt disk, taken from ref. [42], are given for comparison.

W electrode	**Tafel slope / mV dec^{-1}**		$\boldsymbol{j_{spec}}$ **/** $\mu A\ cm^{-2}_{Pt}$
	Low	**high**	
$Pt/WO_3(0)$-450	-93	-177	27.9
$Pt/WO_3(1)$-480	-210	-210	14.3
$Pt/WO_3(2)$-625	-120	-146	13.0

Similarly to polycrystalline Pt, where Tafel slope changes with ORR overvoltage, we observed gradual change of the Tafel slope, with the only exception of platinized partially oxidized W electrode, where this change is practically negligible. According to Gottesfeld [43] the change of Tafel slope can be understood according to the equation:

$$\frac{d(\log j_k)}{d(E^0 - E)} = \frac{1}{b_{int}} + \frac{1}{1-\theta}\frac{d\theta}{dE} \tag{11}$$

where E^0, b_{int} and θ stand for ORR standard electrode potential, intrinsic Tafel slope value (in this case considered to be −120 mV dec^{-1}) and a surface coverage by oxygen species. As we observed that surface processes related to formation of OH_{ads} and Pt-oxide are not significantly affected by the nature of WO_3 support (Fig. 4, right) it is suggested that deviations of Tafel slope from the values typical for Pt, can be due to the alteration of the reaction mechanism (which introduces a new value of the intrinsic Tafel slope, b_{int}') and the effects of a weakly conductive W-oxide layer, i.e., of additional potential-dependent resistance term, $R(E)$, in Eq. (11) as:

$$\frac{d(\log j_k)}{d(E^0 - E)} = \frac{1}{b_{\text{int}}'} + \frac{1}{1-\theta}\frac{d\theta}{dE} + \frac{1}{R(E)} \quad (12)$$

3.5.2. The effect of Pt loading

In contrast to improved HER/HOR kinetics our results point clearly to a loss of ORR activity upon reduction of Pt loading (Fig. 10). Not only that mass activity of Pt is not increasing as loading/dispersion decreases, as in the case for HER kinetics, but it actually decreases. It should be noted that relatively high Pt loadings were investigated here which are above the ones typically considered for the investigation of supported nanosized Pt catalysts [44,45]. Though diffusion limitations have been reached for all three electrodes, in the case of the lowest Pt loading the regions of kinetic control and mixed kinetics span over 0.8 V wide potential window. It should be noted that previous reports suggested that the use of various interactive Pt supports (such as higher W, Ta, Nb altervalent capacity hypo-d-oxides) should be a route to higher reversibility of oxygen electrode reactions [4] while the kinetics of both hydrogen and oxygen electrode reactions have been improved [4-6, 46,47]. Improved ORR kinetics was ascribed to the presence of oxide on (hypo-d-oxide supported) Pt electrocatalysts, resulting in higher ORR onset potential [4]. Within the Gottesfeld's [43] opinion of ORR kinetics, such interaction can be understood on the basis of altered value of the surface redox potential ($E^o_{\text{Pt(H}_2\text{O)/Pt}-\text{OH}_{\text{ads}}}$) implicitly contained in the θ term of Eq. (11). Namely, the increase of this term allows ORR to be triggered at higher potential (of course, if allowed by ORR activation energy at particular electrode surface).

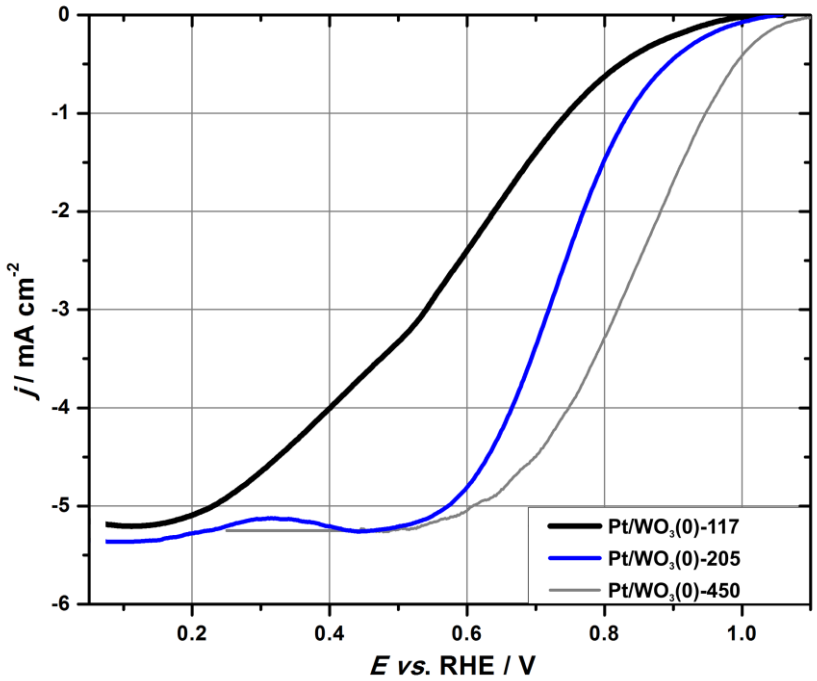

Figure 10. Background-corrected *j-E* curves of oxygen reduction reaction on Pt/WO_3(0)-450, Pt/WO_3(0)-205 and Pt/WO_3(0)-117 composite surfaces, recorded in O_2-saturated 0.1 mol dm^{-3} $HClO_4$ solution at 20 mV s^{-1} using RDE technique (ω = 1400 rpm).

Rather high ORR onset potentials observed, Fig. 9, point to a significant reduction of ORR overvoltage and the approach of ORR onset potential to its thermodynamical value of $E°$ (1.23 V *vs*. RHE). However, it can be unambiguously concluded that there are other processes which hinder ORR once it has been started. This results in an extended region of mixed kinetics, and, consequently, in high value of observed Tafel slopes. We suggested that hindered ORR kinetics is due to the charge transport limitations of oxidized support at high anodic potentials in Pt/WO_3 composite surfaces, when tungsten oxide is in its insulating form. A clear distinction should be made with respect to nanosized Pt/WO_3 catalysts where significant ORR kinetics improvements were observed and to which carbon is added as a current collector enabling efficient charge transport [4,48-50]. In these cases added W-oxide contributes electrocatalytic performances according to the mechanisms discussed above, while carbon, and to some extent metallic Pt component dispersed over support, ensure good conductance of a catalyst layer.

The explanation of the suppressed ORR activity due to the hindered electron transport through the oxide film can also be supported by recent work by Hsu et al. [51]. The authors investigated ORR electrocatalysis by monolayer (ML) Pt deposited over WC support. They claimed that surprisingly low ORR activity of Pt_{ML}/WC surface, compared to massive Pt, is due to the formation of tungsten oxides, as evidenced by XPS. Oxide formation took place both under oxygen atmosphere and deep anodic excursions corresponding to the operating ORR conditions. Although compromited integrity of Pt ML was outlined as the main reason for low ORR activity, observed formation of a non-conductive WO_3 must not be disregarded as a possible reason for low ORR performance.

4. CONCLUSIONS

Potentiodynamic polarization of metallic W disk electrode in pure supporting acidic electrolyte and in Pt plating solutions enabled straightforward control of the oxide thickness on tungsten support and the amount of Pt loaded on the electrode during the preparation of catalytically active Pt/WO_3 composite surfaces. Scanning electron microscopy revealed that nearly spherical Pt particles formed evenly distributed along the electrode surface.

Upon the extended cycling slight progressive changes of a blank cyclic voltammogram of the Pt/WO_3 electrode were observed. Based on the previous reports it was proposed that W-oxo species, resulting from the dissolution of the support, get deposited over the Pt particle surface. This leads to an altered electrochemical response in the H_{UPD} region and the blockage of the Pt active sites for water discharge at high anodic potentials. However, significant losses of Pt were not observed.

Electrocatalytic performances in both HER/HOR and ORR regions were investigated in acidic solution.

It was concluded that the oxidized W support contributes to HER/HOR kinetics at cathodic potentials, which intensifies with the reduction of Pt loading. That is attributed to the hydrogen bronze formation supplemented to the hydrogen spillover.

High ORR onset potentials were observed, approaching the thermodynamic limit of 1.23 V *vs*. RHE, however, low conductivity of the oxidized W support at high anodic potentials resulted in the

extended region of the mixed ORR kinetics for several hundredths of mV. The activity decreased with the reduction of Pt loading.

Presented investigations offer new insights in the ways to modify catalytic activity of platinum by the interactive support, which can be used in the development of new superior Pt-based electrocatalysts.

ACKNOWLEDGEMENT
This work was supported by The Ministry of Education, Science and Technological Development of Republic Serbia through the Project No. III 45014. Financial support provided through the NATO Project EAP.SFPP 984925 - "DURAPEM - Novel Materials for Durable Proton Exchange Membrane Fuel Cells" is also acknowledged. S.M. acknowledges the financial support provided by the Serbian Academy of Sciences and Arts, through the project F-190, "Electrocatalysis in the contemporary processes of energy conversion".

References

1. K. Kinoshita, *J. Electrochem. Soc*., 137 (1990) 845.
2. V. R. Stamenkovic, B. Fowler, B. S. Mun, G. Wang, P. N. Ross, C. A. Lucas and N. M. Marković, *Science* 315 (2007) 493.
3. N. M. Marković and P. N. Ross, *Electrochim. Acta,* 45 (2000) 4101.
4. G. D. Papakonstantinou, J. M. Jaksic, D. Labou, A. Siokou and M. M. Jaksic, *Adv. Phys. Chem.* (2011) Article ID 412165, doi:10.1155/2011/412165.
5. J. M. Jaksic, D. Labou, G. D. Papakonstantinou, A. Siokou and M. M. Jaksic, *J. Phys. Chem. C*, 114 (2010) 18298.
6. N. V. Krstajic, L.M. Vracar, V. R. Radmilovic, S. G. Neophytides, M. Labou, J. M. Jaksic, R. Tunold, P. Falaras and M. M. Jaksic, *Surf. Sci.*, 601 (2007) 1949.
7. S.A.Abbaro, A.C.C.Tseung and D.B.Hibbert , *J. Electrochem. Soc*., 127 (1980) 1106-1107
8. H. W. Kohn and M. Boudart, 145 (1964) 149.
9. N. Muthuramana, P. Kalaignan Guruvaiaha and P. Gnanabaskara Agneeswara, *Materials Chemistry and Physics*, 133 (2012) 924– 931
10. X. Cui, L. Guo, F. Cui, Q. He and J. Shi, J. *Phys. Chem. C*, 113 (2009) 4134.
11. P. K. Shen, K. Y. Chen and A. C. C. Tseung, *J. Electrochem. Soc*., 142 (1995) L85.
12. S. Jayaraman, T. F. Jaramillo, S. H. Baeck and E. W. McFarland, *J. Phys. Chem. B*, 109 (2005) 22958.
13. P. K. Shen and A. C. C. Tseung, *J. Electrochem. Soc*., 141 (1994) 3082.
14. M. Anik and K. Osseo-Asare, *J. Electrochem. Soc*., 149 (2002) B224.
15. A. C. C. Tseung and K. Y. Chen, *Catal. Today*, 38 (1997) 439.
16. D. V. Esposito and J. G. Chen, *Energy Environ. Sci.*, 4 (2011) 3900.
17. D. V. Esposito, S. T. Hunt, A. L. Stottlemyer, K. D. Dobson, B. E. McCandless, R. W. Birkmire and J. G. Chen, *Angew. Chem. Int. Ed.*, 49 (2010) 9859.
18. Y. Liu and W. E. Mustain, *Int. J. Hydrogen Energy*, 37 (2012) 8929.
19. V. M. Nikolic, D. L. Zugic, I. M. Perovic, A. B. Saponjic, B. M. Babic, I. A. Pasti and M. P. Marceta Kaninski, *Int. J. Hydrogen Energy*, 38 (2013) 11340.
20. C. Ma, T. Liu and L. Chen, *Appl. Surf. Sci.*, 256 (2010) 7400.
21. D. D. Vasić, I. A. Pašti and S. V. Mentus, *Int. J. Hydrogen Energy*, 38 (2013) 5009.
22. D. D. Vasić Anićijević, V. M. Nikolić, M. P. Marčeta-Kaninski and I. A. Pašti, *Int. J. Hydrogen Energy*, 38 (2013) 16071.

23. Y. Liu and W. E. Mustain, *ACS Catal.*, 1 (2011) 212.
24. Y. Liu, S. Shrestha and W. E. Mustain, *ACS Catal.*, 2 (2012) 456.
25. S. V. Mentus, *Electrochim Acta*, 50 (2005) 3609.
26. I. Boskovic, S.V. Mentus and M. Pjescic, *Electrochim. Acta*, 51 (2006) 2793.
27. D. Jašin, A. Abu-Rabi, S. Mentus and D. Jovanović, *Electrochim. Acta*, 52 (2007) 4581.
28. S. Mentus, A. Abu Rabi and D. Jašin, *Electrochim. Acta* 69 (2012) 174.
29. P. I. Ortiz, M. L. Teijelo and M. C. Giordano, *J. Electroanal. Chem. Interfacial Electrochem*., 243 (1988) 379.
30. G. Kelsey, *J. Electrochem. Soc.*, 124 (1977) 814.
31. I. A. Pašti, T. Lazarević-Pašti and S. V. Mentus, *J. Electroanal. Chem.*, 665 (2012) 83.
32. C. O. A. Olsson, M. G. Verge and D. Landolt, *J. Eelectrochem. Soc*., 151 (2004) B652.
33. P. J. Kulesza and L. R. Faulkner, *J. Am. Chem. Soc*., 110 (1988) 4905.
34. S. Martínez, M. E. Martins and C. F. Zinola, *Int. J. Hydrogen Energy*, 35 (2010) 5343.
35. A.J. Bard and L.R. Faulkner, Electrochemical Methods: Fundamentals and Applications, John Wiley & Sons, New York, 2001, p. 339.
36. P.M. Quaino, M.R. Gennero de Chialvo and A.C. Chialvo, *Electrochim. Acta*, 52 (2007) 7396–7403
37. W. Sheng, H.A. Gasteiger and Y. Shao-Horn, *J. Electrochem. Soc*., 157 (2010) 1529.
38. R. Notoya and A. Matsuda, *J. Phys. Chem*., 93 (1989) 5521-5523,
39. J. Maruyama, M. Inaba, K. Katakura, Z. Ogumi and Z.-I. Takehara, *J. Electroanal. Chem*., 447 (1998) 201.
40. N. M. Marković, B. N. Grgur and P. N. Ross, *J. Phys. Chem. B*, 101 (1997) 5405.
41. R. M. Q. Mello and E. A. Ticianelli, *Electrochim. Acta*, 42 (1997) 1031.
42. I. A. Pasti, N. M. Gavrilov and S. V. Mentus, *Int. J. Electrochem. Sci.*, 7 (2012) 11076.
43. S. Gottesfeld, Electrocatalysis of oxygen reduction in polymer electrolyte fuel cells: A brief history and a critical examination of present theory and diagnostics, In: M. Koper (Ed.), *Fuel cell catalysis: A surface science approach*, John Wiley and Sons, (2009) New Jersey, p. 1-30.
44. M. Arenz and N.M. Markovic, Half-cell investigations of cathode catalysts for PEM Fuel Cells: From model systems to high-surface-area catalysts, In: *Fuel cell science: Theory, Fundamentals, and Biocatalysis*; A. Wieckowski, J. Nørskov, (Eds.) John Wiley and Sons, (2010) New Jersey,
45. N. Gavrilov, M. Dašić-Tomić, I. Pašti, G. Ciric-Marjanovic and S. Mentus, *Mater. Lett*., 65 (2011) 962.
46. J. M. Jaksic, N. V. Krstajic, L. M. Vracar, S. G. Neophytides, D. Labou, P. Falaras and M. M. Jaksic, *Electrochim. Acta*, 53 (2007) 349.
47. J. M. Jaksic, D. Labou, C. M. Lacnjevac, A. Siokou and M. M. Jaksic, *Appl. Catal. A*, 380 (2010) 1.
48. J. Shim, C.-R. Lee, H.-K. Lee, J.-S. Lee and E. J. Cairns, *J. Power Sources* 102 (2001) 172.
49. D. Y. Zhang, Z. F. Ma, G. X. Wang, K. Konstantinov, X. X. Yuan and H. K. Liu, *Electrochem. Solid-State Lett*., 9 (2006) A423.
50. Z. Yan, W. Wei, J. Xie, S. Meng, X. Lü and J. Zhu, *J. Power Sources*, 222 (2013) 218.
51. I. J. Hsu, Y. C. Kimmel, Y. Dai, S. Chen and J. G. Chen, *J. Power Sources*, 199 (2012) 46.